ACS MATERIALS Au
AN OPEN ACCESS JOURNAL OF THE AMERICAN CHEMICAL SOCIETY



pubs.acs.org/materialsau
Article

# Scalable Manufacturing of Large-Area Pressure Sensor Array for Sitting Posture Recognition in Real Time

*Published as part of the ACS Materials Au virtual special issue "2023 Rising Stars".*

Lu Zheng,‖ Xuemin Hou,‖ Manzhang Xu, Yabao Yang, Jiuwei Gao, Lei Luo, Qixuan Zhu, Weiwei Li,* and Xuewen Wang*

Cite This: ACS Mater. Au 2023, 3, 669−677
Read Online
ACCESS | Metrics & More | Article Recommendations | Supporting Information

**ABSTRACT:** Pressure sensors are considered the key technology for potential applications in real-time health monitoring, artificial electronic skins, and human−machine interfaces. Despite the significant progress in developing novel sensitive materials and constructing unique sensor structures, it remains challenging to fabricate large-area pressure sensor arrays due to the involvement of complex procedures including photolithography, laser writing, or coating. Herein, a scalable manufacturing approach for the realization of pressure sensor arrays with substantially enlarged sensitive areas is proposed using a versatile screen-printing technique. A compensation mechanism is introduced into the printing process to ensure the precise alignment of conductive electrodes, insulation layers, and sensitive microstructures with an alignment error of less than 4 $\mu$m. The fully screen-printed sensors exhibit excellent collective sensing performance, such as a reasonable pressure sensitivity of −2.2 kPa$^{-1}$, a fast response time of 40 ms, and superior durability over 3000 consecutive pressures. Additionally, an integrated 16 × 32 pressure sensor array with a sensing area of 190 × 380 mm$^2$ is demonstrated to precisely recognize the sitting postures and the body weights, showing great potential in continuous and real-time health status monitoring.

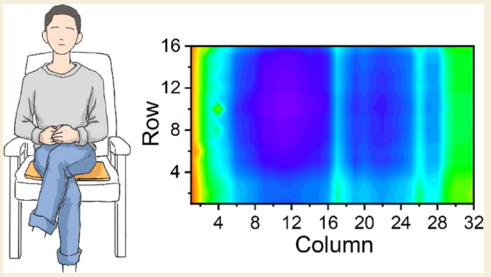


**KEYWORDS:** *pressure sensor array, screen printing, large area, siting posture recognition, compensation mechanism*

## 1. INTRODUCTION

Flexible and wearable electronics have attracted considerable interest in both fundamental research and practical applications in the past decades,[1−4] owing to the miniaturization and convenient integration with sensing networks.[5−7] Particularly, flexible pressure sensors capable of detecting mechanical stimuli are considered the crucial unit and the key technology for potential applications in real-time health monitoring,[8,9] artificial electronic skins,[10−12] and human−machine interfaces[13−15] to name a few. Recently, physical and psychological problems caused by the sedentary lifestyle have recently received special attention. Flexible pressure sensing with array structures provides a non-invasive, seamless, and convenient approach with an intervention function to recognize the sitting postures and correct the wrong sitting states during sustained working or study periods.[16,17] Up to now, significant progress has been made in the development of flexible pressure sensors by exploring novel functional materials,[18−20] introducing unique microstructures,[13,21,22] and constructing unconventional device configurations[23−25] to enhance the collective sensing performance, such as high sensitivity over a wide pressure range, low detection limit, and fast response time.[26] However, the scalable manufacturing of large-area pressure sensors, especially highly integrated sensor arrays, using unconventional materials and device structures remains challenging, yet promising in novel and practical applications including the recognition and correction of sitting postures. The general strategies to realize a pressure sensor array typically include the photolithography technique,[25,27,28] laser writing,[16,26] or drop casting,[22,29,30] which comprises a relatively complex fabrication process. In addition, the sensing areas and sensitive elements are still limited,[16,31−33] which is an obstacle to the precise and accurate monitoring of external stimuli with large sizes or multiple positions.

Screen printing is a versatile technology with the key features of easy operation, cost-effectiveness, and scalability,[34] which is ideal for the manufacturing of flexible electronic devices in large sizes.[35,36] However, several challenges still exist in the employment of screen printing in the realization of multilayer structures including pressure sensor arrays. One key barrier to the achievement of a fully screen-printed presser sensor array is

Received: June 16, 2023
Revised: July 23, 2023
Accepted: July 28, 2023
Published: August 9, 2023

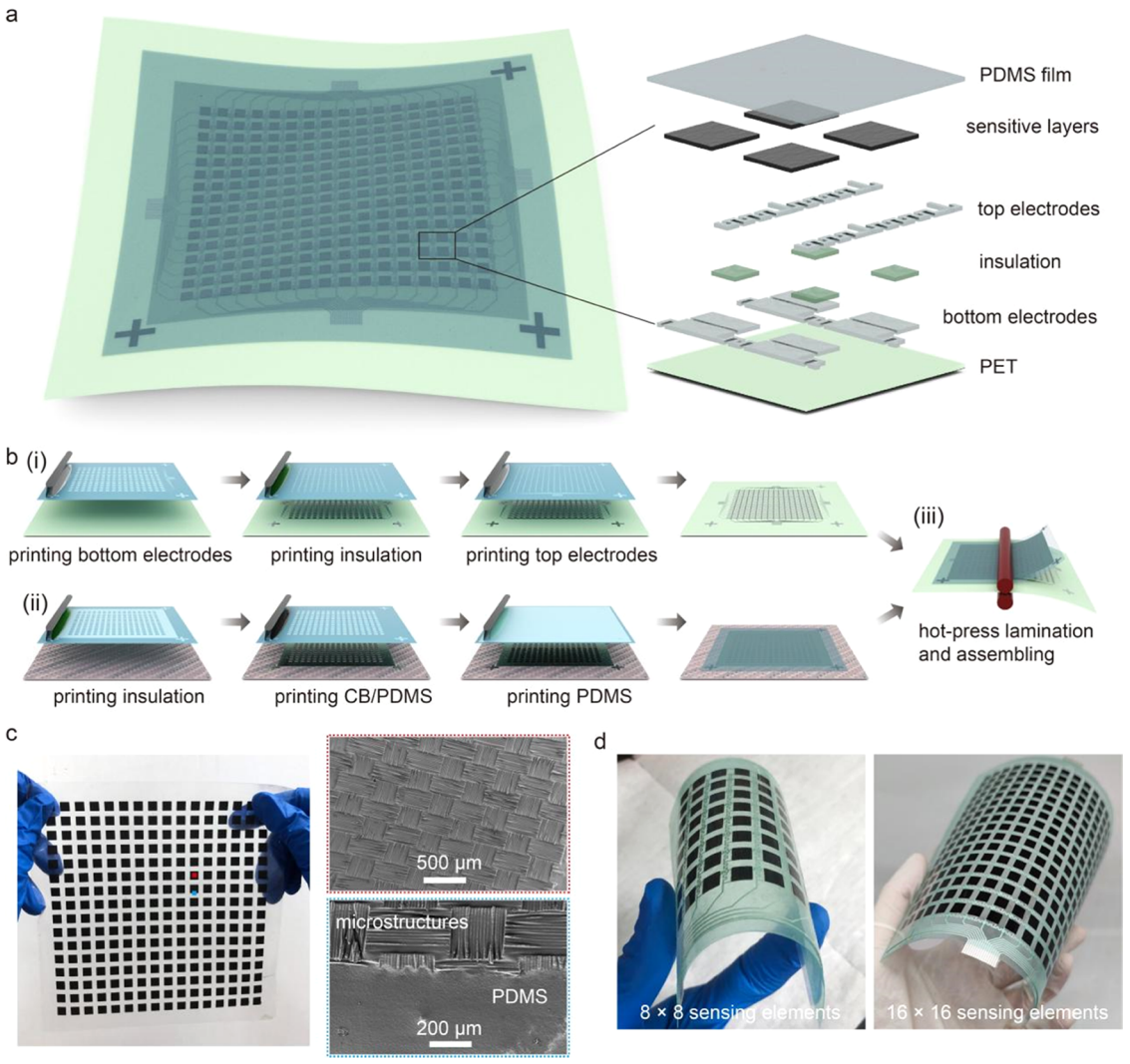


**Figure 1.** Schematic illustration of the designed structure and preparation of large-area pressure sensor array. (a) Conceptual demonstration and exploded view of the sensor array. (b) Schematic of the fabrication process of the sensor array. (c) Photograph and scanning electron microscopy (SEM) image of the sensitive patterns. (d) Photographs of the manufactured sensor array with 8 × 8 and 16 × 16 sensing elements.

the limited accuracy of the alignment between layers, resulting in considerable deviations in the printed patterns. Therefore, it is highly desirable for a significant enhancement in alignment accuracy for the realization of pressure sensor arrays with large areas and low cost toward practical applications in wearable sensing.

Herein, a novel strategy for the scalable manufacturing of large-area pressure sensor arrays is proposed through a full-screen printing process. In the design, both the bottom and top electrodes are printed on one flexible substrate to reduce the overall thickness of the sensor and consequently enhance mechanical flexibility. A compensation mechanism is introduced into the printing process to minimize the alignment errors in the multilayered printing, achieving an alignment resolution of about 4 $\mu$m. The sensor array exhibits high sensitivity over a wide pressure range, fast response time, and low detection limit. A large-area sensor array with 16 × 32 sensing elements is integrated into a cushion to recognize the sitting postures and the pressure distribution of various human weights in real time. This work provides a facile and effective strategy for the realization of large-area pressure sensor arrays toward wearable healthcare electronics for practical applications.

## 2. METHODS

### 2.1. Preparation of Crisscross Electrodes

A poly(ethylene terephthalate) (PET) substrate with a thickness of 200 $\mu$m is cleaned with acetone and ethanol. A commercial silver paste (8000 A, Sunflower Electronics, Inc. Shenzhen) is used for the preparation of conductive electrodes. First, the bottom electrodes are printed on the PET using a dual-servo screen printer (TX-2030ST, Taoxing Printing Inc, Hangzhou) with a screen frame size of 300 mm × 400 mm and a mesh number of 300. After curing at 90 °C for 30 min in an oven, an insulating ink (DHG-9055AD, Qixin Scientific Inc, Shanghai) is printed on the desired position of the bottom electrodes, followed by a cross-linking process under an ultraviolet (UV) light with a wavelength of 365 nm for 3 s. Three printing cycles are conducted to ensure a satisfactory insulating property. Next, the top electrodes are printed using the same conductive ink with optimal curing parameters to complete the fabrication of the crisscross electrodes.

### 2.2. Preparation of Sensitive Films

The composite ink is prepared by adding carbon black (CB) particles with a weight ratio of 8% into poly(dimethylsiloxane) (PDMS),


https://doi.org/10.1021/acsmaterialsau.3c00050
ACS Mater. Au 2023, 3, 669−677

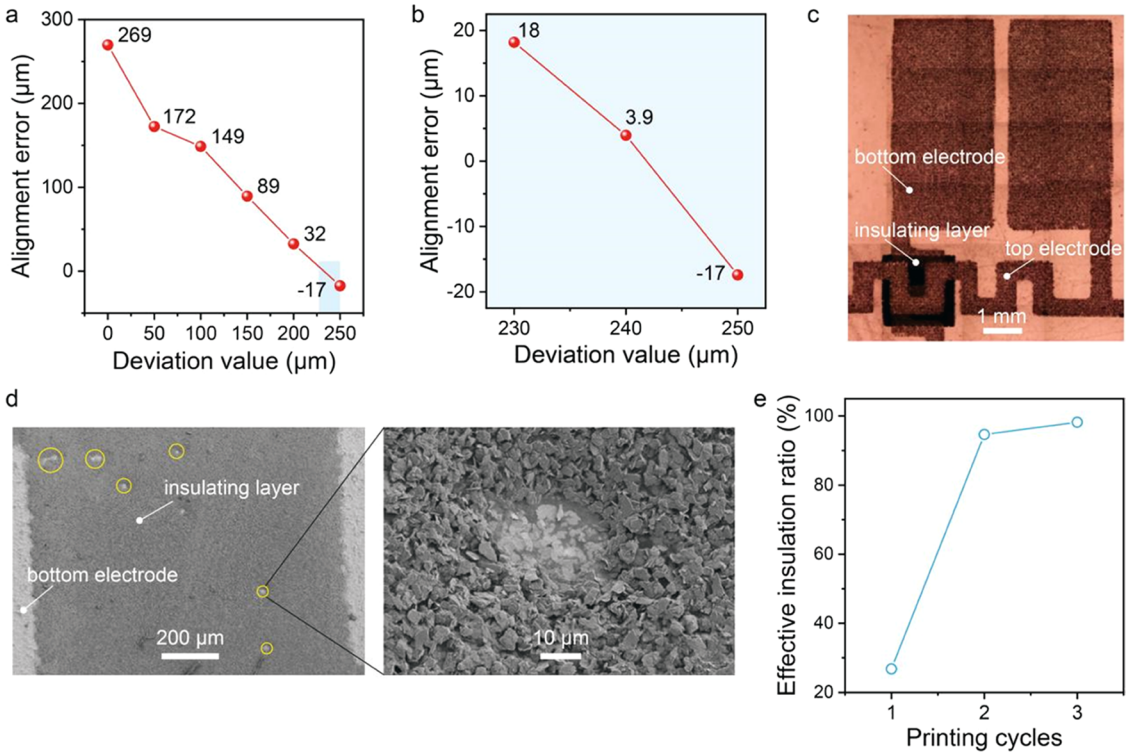


**Figure 2.** Printing alignment and insulating property of the sensor array. (a) Alignment errors as a function of deviation values after the introduction of the compensation mechanism. (b) Alignment errors of the printed patterns with a deviation value of 10 $\mu$m. (c) Optical image of the aligned patterns with an insulation layer sandwiched between the bottom and top electrodes. (d) SEM images of the printed insulation layer for a single printing cycle showing several voids. (e) Effective insulation ratio of the bottom and top electrodes with cyclic printing of insulation layers.

followed by a mixture using a magnetic stirrer for 1 h. Then, the ink is printed onto the surface of a waterproof textile using a stainless steel mesh, followed by a heating process at 70 °C for 2 h to cure the PDMS into a film. Next, a pure PDMS is printed on the surface of the textile and cured at 60 °C for 3 h. Finally, the cured PDMS is peeled off from the textile to obtain the sensitive film with microstructures.

### 2.3. Lamination and Assembling

The PDMS is printed on the surface of conductive electrodes, followed by curing at 60 °C for 20 min to obtain a semi-cured PDMS, which is used as a binder. Then, the sensitive film is aligned with the electrodes and laminated using a rolling approach to complete the manufacturing of the sensor array. It should be noted that there have cross cursors on the electrode layer and sensitive layer, which are used to align different layers by placing the centers at the coincident positions with the assistance of a microscope. Using the proposed approach, the electrode layer and sensitive layer are aligned in the lamination and assembling process.

### 2.4. Characterization

A field emission electron microscopy microscope (Zeiss) is used to investigate the printed insulators and the microstructures of the sensitive film. The optical images are taken by optical microscopy (Nexcope NMM910). A homemade field programmable gate array (FPGA) system is utilized to collect and analyze the data from the pressure array. The hardware of the system mainly includes a data acquisition unit (PXI-6289), a multichannel gate unit (PXI-2602, Altay), and a controller (PXI-7685, Altay). The upper-computer software is realized using Labview.

## 3. RESULTS AND DISCUSSION

### 3.1. Design Concept and Fabrication of the Pressure Sensor Array

Figure 1a shows the concept and device structure of the large-area pressure sensor array, which consists of crisscross electrodes, insulation layers, and sensitive layers (detailed parameters in Figure S1, Supporting Information). There are several advantages of the proposed design. In contrast to the conventional pressure sensors with separate electrodes on two substrates to form sandwich structures,[37] the crisscross electrodes in our design are printed on one flexible substrate, providing the capability to reduce the thickness of the overall sensor and consequently enhance mechanical flexibility. In addition, high integration level of the sensing elements is achieved by significantly reducing the number of leads to 32 compared to a value of 512 for separate designs of elements. Moreover, the sensor array is highly compact, which is beneficial for miniaturization. The working principle of the proposed sensor array is based on the resistive change between two parallel electrodes (Figure S2, Supporting Information). Specifically, the microstructures on the surface of the sensing patterns are deformed when an external force is applied to the device, resulting in an enlarged interface. The variable contact areas of sensing patterns and the conductive electrodes under pressure allow for more electrical pathways, which lowers the contact resistance.

The proposed strategy to fabricate the sensor array is schematically illustrated in Figure 1b, which involves three major steps: printing of crisscross electrodes, patterning of sensing elements, and device lamination. First, bottom electrodes are screen-printed onto a flexible poly(ethylene terephthalate) (PET) substrate (thickness of 200 $\mu$m) using a commercial Ag flake ink with optimized printing parameters (see details in Section 2). After curing at 90 °C for 30 min, the printed electrodes are partially covered by an insulation layer to prevent the short between the top and bottom electrodes. Then, the top electrodes are printed after rotating the substrate


https://doi.org/10.1021/acsmaterialsau.3c00050
ACS Mater. Au 2023, 3, 669−677

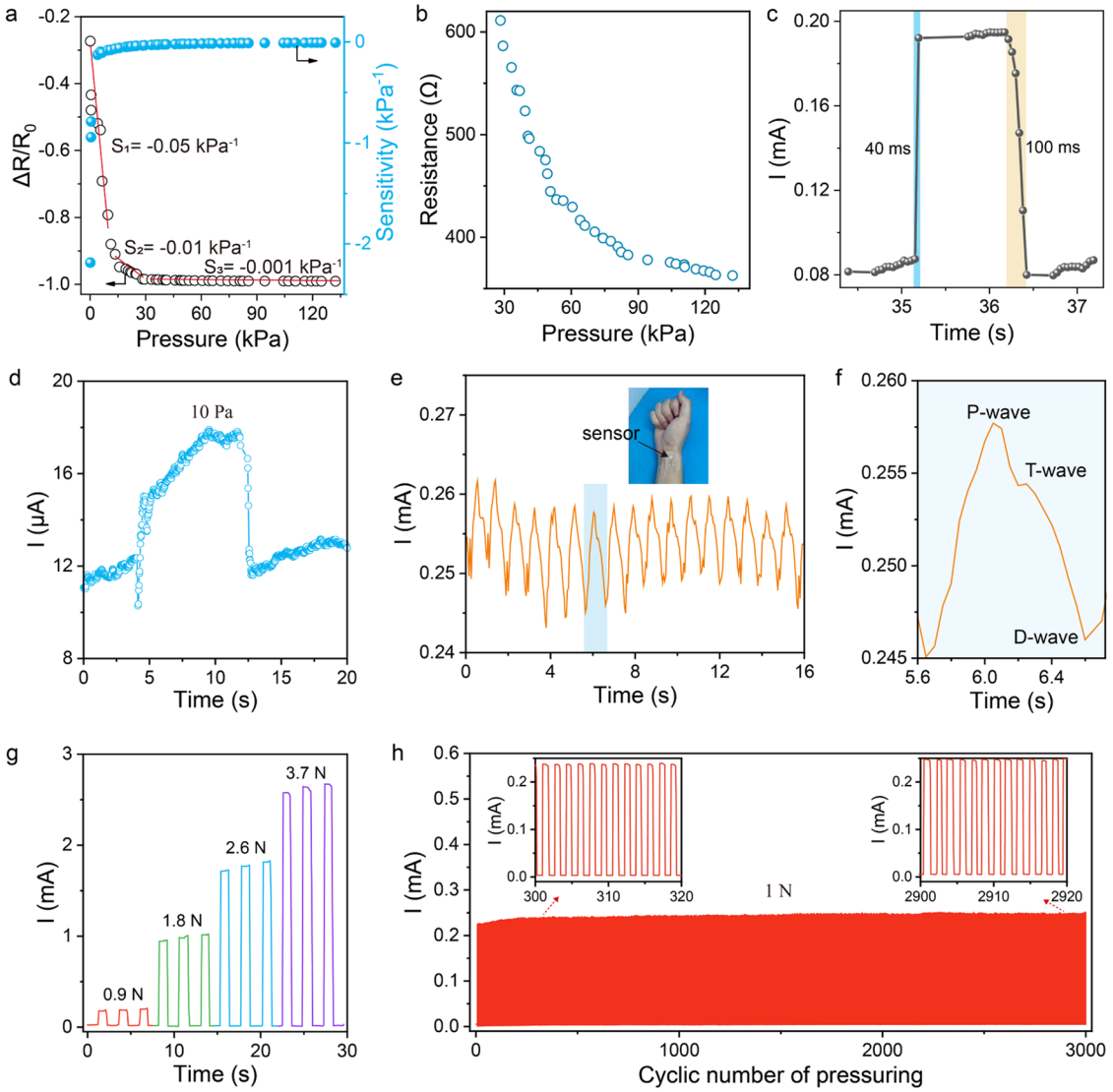


**Figure 3.** Sensing properties of the fully screen-printed pressure sensor. (a) Relative resistance variation and calculated pressure sensitivity as a function of pressure up to 132 kPa. (b) Resistance variation in response to applied pressure from 30 to 132 kPa. (c) Response and recovery time of the pressure sensor to an applied force of about 1 N. (d) Real-time response to a metal ball showing a detection limit of 10 Pa. (e) Output signals of the pressure sensor in monitoring arterial pulse waves captured within 16 s. Inset is a photograph showing the sensor attached to a human wrist. (f) Extracted single pulse wave showing distinct systolic and diastolic peaks noted by percussion wave (P-wave), tidal wave (T-wave), and diastolic wave (D-wave), respectively. (g) Output current of a pressure sensor in response to various forces from 0.9 to 3.7 N. (h) Output current of the pressure sensor under repeated loading/unloading cycles under a force of 1 N.

for 90°, followed by a curing process to complete the fabrication of the electrodes. For the sensing patterns, a carbon black (CB) and poly(dimethylsiloxane) (PDMS) composite ink with a CB weight ratio of 8% is screen-printed onto a clean waterproof textile to duplicate the microstructures on the textile. Next, a thin PDMS layer is printed onto the sensitive patterns to form a cross-linked thin layer, which allows the delamination of the sensing film from the textile (Figure 1b). Figure 1c shows the scanning electron microscopy (SEM) images of the microstructures of the sensitive pattern, comprising periodic strip lines with anisotropic structures, which ensures a uniform and consistent response under eternal forces from different pressing directions. Finally, the electrodes and the sensing films are laminated and assembled via hot pressing to complete the fabrication of the sensor array. Using the proposed strategy, large-area pressure sensor arrays can be manufactured. Figure 1d shows two photographs of the flexible pressure sensor arrays with sensing elements of 8 × 8, 16 × 16, and 16 × 32, demonstrating a scalable process, which is of significant importance for the potential applications of pressure sensors.

It is well known that alignment is the key challenge for multilayer printing. In a screen printing process, the screen mesh has a micro deformation in the printing direction due to the applied pressure force and tensile force by the squeegee (Figure S3a, Supporting Information). Therefore, the printed patterns have a displacement along the printing direction compared to the viewing patterns from a microscope (Figure S3b, Supporting Information), resulting in an alignment error. As shown in Figure 2a, there has an alignment error of about 270 $\mu$m when the patterns on the screen mesh are aligned to the desired position on the substrate by observing from the optical microscope, which leads to the electrical short of the crisscross electrodes due to the uncovered insulators on the


https://doi.org/10.1021/acsmaterialsau.3c00050
ACS Mater. Au 2023, 3, 669−677

bottom electrodes. To solve this issue, we develop a compensation approach to introduce an additional displacement to the substrates by regulating the micrometer knob equipped in the screen printer. Specifically, the substrates with the printed electrodes are gradually shifted along the moving direction of the squeegee. Initially, a deviation value of 50 $\mu$m is applied to the substrates. As shown in Figure 2a, the alignment error is gradually reduced with the increasing of the additional displacement. Note that the alignment error becomes negative when the substrate is shifted with a value of 250 $\mu$m, indicating that the deviation is beyond the reasonable range. We then change the deviation value from 50 to 10 $\mu$m. As expected, a minimum alignment error of 3.95 $\mu$m is achieved when the deviation value is 240 $\mu$m (Figure 2b), which is sufficient for precise alignment of multilayer printing (Figure 2c).

In addition to the alignment error, the insulating property of the insulation layers is another key issue in the proposed structure and the printing process. This is because the bottom and top electrodes may have possible electrical short due to the connection through the insulators. As shown in Figure 2d, there are many voids in the printed insulators, which are attributed to the unsatisfactory wettability of the insulating ink on the Ag layer. This results in a low effective insulation rate (Figure 2e). To solve this issue, the insulating ink is printed for several cycles, followed by treatment under a UV light for cross-linking and polymerization. It is found that three printing cycles are sufficient to ensure that the printed electrodes are successfully insulated with an effective insulation rate of 100%, which has been verified by the zero current between the top and bottom electrodes (Figure S4, Supporting Information).

### 3.2. Electrical Output and Sensing Performance

After the fabrication of the sensor array, we evaluate the sensing properties, including the sensitivity, response time, and detection limit. To evaluate the response of the proposed pressure sensor under static and dynamic forces, a voltage of 1 V is applied to the sensor and the resistance change under different pressure is recorded by a multimeter. As shown in Figure 3a, the resistance decreases within a static pressure up to 132 kPa. Specifically, there is a sharp decrease in resistance when a pressure less than 30 kPa is applied to the sensor due to the significant enhancement of the contact areas between the sensing microstructures and the electrodes. At a pressure larger than 30 kPa, the resistance gradually decreases because of the minimal change in the contact density. Despite the relatively small change in resistance, the larger pressures are precisely detected (Figure 3b). The sensitivity ($S$) of a resistive pressure sensor is typically defined as $S = \delta(\Delta R/R_0)/\delta P$,[13] where $R_0$ is the initial resistance before force loading, and $\Delta R = R - R_0$ refers to the variation of the resistance under an applied pressure of $P$. The sensitivity value can be obtained from the slope of the resistance versus pressure in the fitted curve. In the low pressure range (<10 kPa), the sensor exhibits a fitted sensitivity of 0.05 kPa$^{-1}$. At pressures between 10 and 30 kPa, the sensitivity dropped to 0.01 kPa$^{-1}$, while the value further abruptly decreases to 0.0001 kPa$^{-1}$ under pressures larger than 30 kPa due to the considerable flatness of the microstructures. These sensitivity values are close to or higher than several representative capacitive and resistive pressure sensors in the literature (Table S1).[37−39] The sensitivity at each pressure has also been calculated, revealing a power law dependence. It is observed that the sensitivity gradually decreases from −2.2 to −0.007 kPa$^{-1}$ with the increase in pressure (Figure 3a), which is consistent with the slope of the fitted curve. It is worth noting that such progressive sensitivities allow for the precise detection of low force loading and the capability for monitoring higher pressures, which is desirable for potential applications in sitting posture recognition.

A fast response speed is essential for pressure sensors in the real-time detection of applied pressure. It is well established that the introduction of microstructures to the sensitive layer is beneficial for a reduction in the response time to the applied forces due to the rapid energy storage and release. Here, the sensitive layers contain strip-line microstructures with anisotropic patterns, which is effective to reduce the response and recovery time. As shown in Figure 3c, the fabricated sensor responds rapidly to a force of about 1 N with a rising time and recovery time of 40 and 100 ms, respectively, ensuring an immediate response to external forces. The detection limit is another important parameter of a pressure sensor, which has been further investigated by loading a metallic particle with a weight of about 0.25 g to the surface of the pressure sensor. The output current increases abruptly from 12 $\mu$A to about 18 $\mu$A after loading the particle (Figure 3d), indicating a calculated detection limit of about 10 Pa. When the particle is removed, the current recoveries to 12 $\mu$A. The pressure sensor is then firmly attached to a human wrist using a double-sided polyurethane (PU) tape to monitor the pulse wave, which is not easy for most reported pressure sensors.[13,25,40] Despite the slight fluctuation in the output current of the pressure sensor, stable and precise recording of the pulse conductions is achieved for several cycles (Figure 3e), confirming the high sensitivity and low detection limit of the pressure sensor. Note that the introduction of a PU tape benefits the signal accuracy (Figure S5, Supporting Information) due to the strong attachment of the sensor to a human wrist. The extracted pulse waveform from one pulse clearly shows some amplitude features such as the systolic and diastolic peaks (Figure 3f), providing a reliable and real-time method to monitor human health for early disease diagnosis. Therefore, the pressure sensor has the potential in detecting tiny variations of pressure to be used in wearable electronics and human−machine interaction systems.

For the dynamic response, the resistance changes of the pressure sensor are recorded after varying the applied forces from 0.9 to 3.7 N. The current response is constant under a fixed force for three cycles of loading and unloading, whereas the current recovers to nearly zero after the force is removed (Figure 3g). In addition, the responding output of current signals increases with increasing force, indicating an accurate response to external force and reliable stability over a broad force range. The long-term durability pressure perception is further verified through cyclic loading/unloading under an external force of 1 N at 0.7 Hz. There is no significant variation in output currents with negligible drift or fluctuation throughout the 3000 compression-release cycles (Figure 3h), indicating excellent stability and repeatability of the pressure sensor. These features are highly desirable for the sensitive, real-time, and reliable transduction of pressure signals.

### 3.3. Real-Time Monitoring of Sitting Postures

Taking the advantages of high sensitivity and fast response over a wide pressure range, the large-area pressure sensor array has been integrated with a cushion to record the pressure distribution of a human with diverse sitting postures in real


https://doi.org/10.1021/acsmaterialsau.3c00050
ACS Mater. Au 2023, 3, 669−677

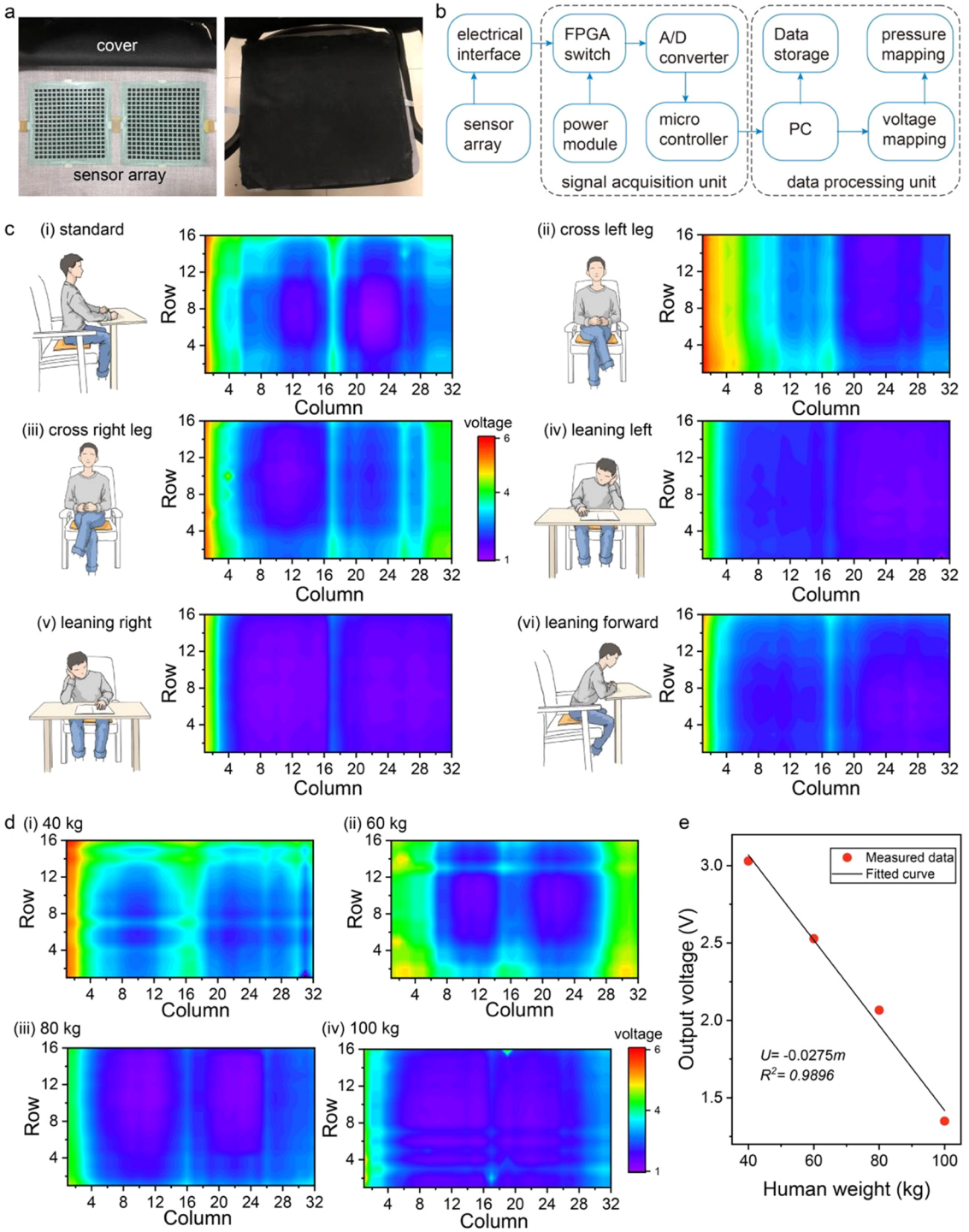


**Figure 4.** Demonstration of the large-area sensor array for siting posture recognition. (a) Photographs of the 16 × 32 sensor array and the integrated cushion. (b) Hardware architecture of the FPGA system with functions of data acquisition, processing, display, and storage. (c) Output voltages with respect to the changes in sitting postures. (d) Contour plots of pressure distribution for humans with different body weights at standard sitting posture. (e) Relationship between output voltage and body weights.

time. Two sensor arrays with 16 × 16 sensing elements are bridged and connected with flexible flat cables to form a larger array with a sensing area of 190 × 380 $mm^2$ (Figure 4a), which is sufficient to cover the pressure distribution of the sitting postures of an adult. Note that the sensing elements are two orders of magnitude more and the sensor array is at least two times larger as compared to previous pressure arrays (Table S1), benefiting the high-accuracy recording of pressure signals.

To achieve a real-time collection and transduction of pressure distribution, we construct a customized field programmable gate array (FPGA) data analysis system (Figure 4b). A flexible electrical interface is utilized to connect with the sensor array to collect signal variation in the sensor array. Then, an FPGA was implemented to acquire the voltage data by controlling a gate unit via a switch, followed by the data transduction to an analog-to-digital converter (A/D) to convert the voltage into


https://doi.org/10.1021/acsmaterialsau.3c00050
ACS Mater. Au 2023, 3, 669−677

digital format. Next, a microcontroller is used to send the converted data to a processing and analysis unit. The processed data of all the sensing elements are displayed on a screen in the form of two-dimensional mapping. The pressure distribution of a crisscross sensor up to 32 × 32 sensing elements can be accurately recorded and analyzed in real time due to a processing time of less than 1 ms for a single element, ensuring the real-time display of the pressure mapping of the 16 × 32 sensor array. By considering the potential health risks to young kids and office workers, a total of six common sitting postures are selected, including straight sitting, crossed legs, leaning postures, and forward sitting. As shown in Figure 4c, the postures are clearly distinguished by visualizing the pressure mapping. Specifically, the pressure distribution of the normal sitting is similar at both sides of the sensor array, indicating that there is no obvious difference in pressure for the ischium when the truck states are straight. Since our sensor array is large enough to cover the sitting areas, the pressures at distinct parts of the body can be recognized (Figure 4c,i). The elliptic areas indicate a larger pressure than that of the bottom areas, assigning to the ischium and thighs, respectively, which is roughly consistent with the real loading features of normal sitting. In contrast, the sensor array exhibits distinct signals when the user is in poor sitting postures, such as sitting with leg up, leaning states, and sitting forward. These sitting states have been precisely recorded and displayed in the pressure mappings (Figure 4c,ii–vi), which can be used for monitoring and preventing humpback and other related health risks. In addition to the recognition of sitting gestures, the pressure sensor is also beneficial to identify the pressure distribution of different weights because of the large sensing range. Four volunteers with body weights of about 40, 60, 80, and 100 kg sit on the cushion, and the pressure distributions are recorded. It is observed that the blue and purple areas in the pressure mapping are expanding with the increase in body weights (Figure 4d), revealing that the contact areas and pressures with the cushion are enlarged. The linear relationship between the output voltage ($U$) with the weight ($m$) provides a value $U$ of −0.0275 m (Figure 4e), which can be used to predict the output signals for various body weights. It should be noted that the output voltages at the side areas (i.e., columns 1 and 2) are relatively larger than that of the right side in some contour plots, indicating a smaller pressure distribution, which can be attributed to the sitting positions of the volunteer. As mentioned, the combined fast speed of the sensor response and the data acquisition system is expected to demonstrate immense potential in health risk monitoring, especially in the real-time recognition and correction of poor sitting postures.

## 4. SUMMARY AND CONCLUSIONS

In this study, a multilayered design is used for the realization of a pressure sensor array and for the integration with a cushion to recognize and correct the sitting postures in real time. A versatile screen printing is utilized for the scalable manufacturing of the large-area multilayer structure by introducing a compensation mechanism into the alignment process. Our strategy minimizes the deviation errors and achieves a printing resolution of about 4 $\mu$m, which significantly improves the printing accuracy. Moreover, sensitive patterns with microstructures on the surface are also printed using an optimal CB/PDMS composite ink to boost the sensing performance. As expected, the fabricated pressure sensor exhibits a high-pressure sensitivity, a fast response, a low detect limit, and a wide sensing range. Together with a customized FPGA unit with a data acquisition time of 1 ms for a single element, a flexible sensing system can precisely detect the variation in the output signal of the large-are sensor array and display the pressure mapping without delay. We believe that the proposed approach opens a unique route for large-area manufacturing of flexible sensors with arrayed structures, which is expected to expand the practical applications of pressure sensor array, such as diagnosing cardiovascular disease by recording pulse wave velocity, monitoring sound signals, interacting with the machine through a human–machine interface, and measuring parameters of aircraft.

## ■ ASSOCIATED CONTENT

### Data Availability Statement

The data underlying this study will be made openly available at the time of publication of the article in the NOMAD repository at.

### Supporting Information

The Supporting Information is available free of charge at https://pubs.acs.org/doi/10.1021/acsmaterialsau.3c00050.

Design concept and detailed parameters of the sensor array; illustrations of the working principles and screen printing process; pulse wave for the sensor without adhesive tape; comparison table for the sensor array and published papers (PDF)

## ■ AUTHOR INFORMATION


### Corresponding Authors

**Weiwei Li** − *Frontiers Science Center for Flexible Electronics & Institute of Flexible Electronics, Northwestern Polytechnical University, Xi'an 710072, China*; Email: iamwwli@nwpu.edu.cn

**Xuewen Wang** − *Frontiers Science Center for Flexible Electronics & Institute of Flexible Electronics, Northwestern Polytechnical University, Xi'an 710072, China; Shaanxi Key Laboratory of Flexible Electronics (KLoFE) and MIIT Key Laboratory of Flexible Electronics (KLoFE), Northwestern Polytechnical University (NPU), Xi'an 710072, China;* orcid.org/0000-0002-9689-6678; Email: iamxwwang@nwpu.edu.cn

### Authors

**Lu Zheng** − *Frontiers Science Center for Flexible Electronics & Institute of Flexible Electronics, Northwestern Polytechnical University, Xi'an 710072, China*

**Xuemin Hou** − *Frontiers Science Center for Flexible Electronics & Institute of Flexible Electronics, Northwestern Polytechnical University, Xi'an 710072, China*

**Manzhang Xu** − *Frontiers Science Center for Flexible Electronics & Institute of Flexible Electronics, Northwestern Polytechnical University, Xi'an 710072, China;* orcid.org/0000-0001-6752-5299

**Yabao Yang** − *Frontiers Science Center for Flexible Electronics & Institute of Flexible Electronics, Northwestern Polytechnical University, Xi'an 710072, China*

**Jiuwei Gao** − *Frontiers Science Center for Flexible Electronics & Institute of Flexible Electronics, Northwestern Polytechnical University, Xi'an 710072, China*




https://doi.org/10.1021/acsmaterialsau.3c00050
ACS Mater. Au 2023, 3, 669–677

**Lei Luo** − *Frontiers Science Center for Flexible Electronics & Institute of Flexible Electronics, Northwestern Polytechnical University, Xi'an 710072, China*

**Qixuan Zhu** − *Frontiers Science Center for Flexible Electronics & Institute of Flexible Electronics, Northwestern Polytechnical University, Xi'an 710072, China*

Complete contact information is available at: https://pubs.acs.org/10.1021/acsmaterialsau.3c00050

### Author Contributions

[‖]L.Z. and X.H. contributed equally to this work. L.Z. contributed to data curation (lead), methodology (lead), writing-original draft (lead), writing-review & editing (lead); X.H. data curation (lead), formal analysis (lead), investigation (lead), methodology (lead), validation (lead); M.X. contributed to data curation (supporting), visualization (lead); Y.Y. contributed to data curation (equal), formal analysis (supporting), methodology (supporting); J.G. contributed to data curation (supporting), formal analysis (supporting), methodology (supporting); L.L. contributed to data curation (supporting), visualization (supporting); Q.Z. contributed to visualization (equal); W.L. contributed to data curation (lead), methodology (lead), validation (lead), visualization (equal), writing-original draft (lead), writing-review & editing (lead); X.W. contributed to methodology (lead), validation (lead), visualization (supporting), project administration (lead), funding acquisition (lead), writing-original draft (lead), writing-review & editing (lead).

### Notes

The authors declare no competing financial interest.

## ■ ACKNOWLEDGMENTS

This project was supported by the National Key Research and Development Program of China (2020YFB2008501), the National Natural Science Foundation of China (11904289), Key Research and Development Program of Shaanxi Province (2020ZDLGY04-08, 2020GXLH-Z-027), the Natural Science Foundation of Shaanxi Province (2019JQ-613, 2022JQ-659), the Natural Science Foundation of Ningbo (202003N4003), the Fundamental Research Funds for the Central Universities (3102019PY004, 31020190QD010, and 3102019JC004), and the start-up funds from Northwestern Polytechnical University (G2022WD01001).

## ■ REFERENCES

(1) Sani, E. S.; Xu, C.; Wang, C.; Song, Y.; Min, J.; Tu, J.; Solomon, S. A.; Li, J.; Banks, J. L.; Armstrong, D. G.; Gao, W. A stretchable wireless wearable bioelectronic system for multiplexed monitoring and combination treatment of infected chronic wounds. *Sci. Adv.* **2023**, *9*, No. eadf7388.

(2) Lim, H. R.; Kim, H. S.; Qazi, R.; Kwon, Y. T.; Jeong, J. W.; Yeo, W. H. Advanced soft materials, sensor integrations, and applications of wearable flexible hybrid electronics in healthcare, energy, and environment. *Adv. Mater.* **2020**, *32*, No. 1901924.

(3) Ates, H. C.; Nguyen, P. Q.; Gonzalez-Macia, L.; Morales-Narváez, E.; Güder, F.; Collins, J. J.; Dincer, C. End-to-end design of wearable sensors. *Nat. Rev. Mater.* **2022**, *7*, 887−907.

(4) Jiang, H.; Zheng, L.; Liu, Z.; Wang, X. Two-dimensional materials: From mechanical properties to flexible mechanical sensors. *InfoMat* **2020**, *2*, 1077−1094.

(5) Yang, H.; Li, J.; Xiao, X.; Wang, J.; Li, Y.; Li, K.; Li, Z.; Yang, H.; Wang, Q.; Yang, J.; et al. Topographic design in wearable MXene sensors with in-sensor machine learning for full-body avatar reconstruction. *Nat. Commun.* **2022**, *13*, No. 5311.

(6) Meng, K.; Xiao, X.; Wei, W.; Chen, G.; Nashalian, A.; Shen, S.; Xiao, X.; Chen, J. Wearable pressure sensors for pulse wave monitoring. *Adv. Mater.* **2022**, *34*, No. 2109357.

(7) Gao, J.; Fan, Y.; Zhang, Q.; Luo, L.; Hu, X.; Li, Y.; Song, J.; Jiang, H.; Gao, X.; Zheng, L.; et al. Ultra-Robust and Extensible Fibrous Mechanical Sensors for Wearable Smart Healthcare. *Adv. Mater.* **2022**, *34*, No. 2107511.

(8) Sharma, S.; Pradhan, G. B.; Chhetry, A.; Shrestha, K.; Bhatta, T.; Zhang, S.; Kim, D.; Jeong, S.; Shin, Y.; Zahed, M. A.; et al. Graphene-polymer nanocomposites electrode with ionic nanofibrous membrane for highly sensitive supercapacitive pressure sensor. *Nano Today* **2023**, *48*, No. 101698.

(9) Li, Y.; Cui, Y.; Zhang, M.; Li, X.; Li, R.; Si, W.; Sun, Q.; Yu, L.; Huang, C. Ultrasensitive Pressure Sensor Sponge Using Liquid Metal Modulated Nitrogen-Doped Graphene Nanosheets. *Nano Lett.* **2022**, *22*, 2817−2825.

(10) Wu, X.; Khan, Y.; Ting, J.; Zhu, J.; Ono, S.; Zhang, X.; Du, S.; Evans, J. W.; Lu, C.; Arias, A. C. Large-Area Fabrication of High-Performance Flexible and Wearable Pressure Sensors. *Adv. Electron. Mater.* **2020**, *6*, No. 1901310.

(11) Lee, B.; Oh, J.-Y.; Cho, H.; Joo, C. W.; Yoon, H.; Jeong, S.; Oh, E.; Byun, J.; Kim, H.; Lee, S.; et al. Ultraflexible and transparent electroluminescent skin for real-time and super-resolution imaging of pressure distribution. *Nat. Commun.* **2020**, *11*, No. 663.

(12) Chen, J.; Zhu, Y.; Chang, X.; Pan, D.; Song, G.; Guo, Z.; Naik, N. Recent progress in essential functions of soft electronic skin. *Adv. Funct. Mater.* **2021**, *31*, No. 2104686.

(13) Bai, N.; Wang, L.; Xue, Y.; Wang, Y.; Hou, X.; Li, G.; Zhang, Y.; Cai, M.; Zhao, L.; Guan, F.; et al. Graded interlocks for iontronic pressure sensors with high sensitivity and high linearity over a broad range. *ACS Nano* **2022**, *16*, 4338−4347.

(14) He, F.; You, X.; Wang, W.; Bai, T.; Xue, G.; Ye, M. Recent progress in flexible microstructural pressure sensors toward human−machine interaction and healthcare applications. *Small Methods* **2021**, *5*, No. 2001041.

(15) Yin, R.; Wang, D.; Zhao, S.; Lou, Z.; Shen, G. Wearable sensors-enabled human−machine interaction systems: from design to application. *Adv. Funct. Mater.* **2021**, *31*, No. 2008936.

(16) Huang, H.; Dong, Y.; Wan, S.; Shen, J.; Li, C.; Han, L.; Dou, G.; Sun, L. A transient dual-type sensor based on MXene/cellulose nanofibers composite for intelligent sedentary and sitting postures monitoring. *Carbon* **2022**, *200*, 327−336.

(17) Lei, H.; Xiao, J.; Chen, Y.; Jiang, J.; Xu, R.; Wen, Z.; Dong, B.; Sun, X. Bamboo-inspired self-powered triboelectric sensor for touch sensing and sitting posture monitoring. *Nano Energy* **2022**, *91*, No. 106670.

(18) Keum, K.; Eom, J.; Lee, J. H.; Heo, J. S.; Park, S. K.; Kim, Y.-H. Fully-integrated wearable pressure sensor array enabled by highly sensitive textile-based capacitive ionotronic devices. *Nano Energy* **2021**, *79*, No. 105479.

(19) Cao, K.; Wu, M.; Bai, J.; Wen, Z.; Zhang, J.; Wang, T.; Peng, M.; Liu, T.; Jia, Z.; Liang, Z.; Jiang, L. Beyond skin pressure sensing: 3D printed laminated graphene pressure sensing material combines extremely low detection limits with wide detection range. *Adv. Funct. Mater.* **2022**, *32*, No. 2202360.

(20) Chen, S.; Fan, S.; Qi, J.; Xiong, Z.; Qiao, Z.; Wu, Z.; Yeo, J. C.; Lim, C. T. Ultrahigh Strain-Insensitive Integrated Hybrid Electronics Using Highly Stretchable Bilayer Liquid Metal Based Conductor. *Adv. Mater.* **2023**, *35*, No. 2208569.

(21) Bai, N.; Wang, L.; Wang, Q.; Deng, J.; Wang, Y.; Lu, P.; Huang, J.; Li, G.; Zhang, Y.; Yang, J.; et al. Graded intrafillable architecture-based iontronic pressure sensor with ultra-broad-range high sensitivity. *Nat. Commun.* **2020**, *11*, No. 209.

(22) Pan, L.; Chortos, A.; Yu, G.; Wang, Y.; Isaacson, S.; Allen, R.; Shi, Y.; Dauskardt, R.; Bao, Z. An ultra-sensitive resistive pressure sensor based on hollow-sphere microstructure induced elasticity in conducting polymer film. *Nat. Commun.* **2014**, *5*, No. 3002.

(23) Wang, H. L.; Kuang, S. Y.; Li, H. Y.; Wang, Z. L.; Zhu, G. Large-area integrated triboelectric sensor array for wireless static and dynamic pressure detection and mapping. *Small* **2020**, *16*, No. 1906352.
(24) Jung, Y.; Choi, J.; Lee, W.; Ko, J. S.; Park, I.; Cho, H. Irregular Microdome Structure-Based Sensitive Pressure Sensor Using Internal Popping of Microspheres. *Adv. Funct. Mater.* **2022**, *32*, No. 2201147.
(25) He, J.; Zhou, R.; Zhang, Y.; Gao, W.; Chen, T.; Mai, W.; Pan, C. Strain-insensitive self-powered tactile sensor arrays based on intrinsically stretchable and patternable ultrathin conformal wrinkled graphene-elastomer composite. *Adv. Funct. Mater.* **2022**, *32*, No. 2107281.
(26) Li, Y.; Wei, Y.; Yang, Y.; Zheng, L.; Luo, L.; Gao, J.; Jiang, H.; Song, J.; Xu, M.; Wang, X.; Huang, W. The Soft-Strain Effect Enabled High-Performance Flexible Pressure Sensor and Its Application in Monitoring Pulse Waves. *Research* **2022**, *2022*, No. 0002.
(27) Song, J.-K.; Son, D.; Kim, J.; Yoo, Y. J.; Lee, G. J.; Wang, L.; Choi, M. K.; Yang, J.; Lee, M.; Do, K.; et al. Wearable Force Touch Sensor Array Using a Flexible and Transparent Electrode. *Adv. Funct. Mater.* **2017**, *27*, No. 1605286.
(28) Park, Y. J.; Sharma, B. K.; Shinde, S. M.; Kim, M.-S.; Jang, B.; Kim, J.-H.; Ahn, J.-H. All MoS2-Based Large Area, Skin-Attachable Active-Matrix Tactile Sensor. *ACS Nano* **2019**, *13*, 3023−3030.
(29) Zhang, Y.; Yang, J.; Hou, X.; Li, G.; Wang, L.; Bai, N.; Cai, M.; Zhao, L.; Wang, Y.; Zhang, J.; et al. Highly stable flexible pressure sensors with a quasi-homogeneous composition and interlinked interfaces. *Nat. Commun.* **2022**, *13*, No. 1317.
(30) Su, X.; Wu, X.; Chen, S.; Nedumaran, A. M.; Stephen, M.; Hou, K.; Czarny, B.; Leong, W. L. A Highly Conducting Polymer for Self-Healable, Printable, and Stretchable Organic Electrochemical Transistor Arrays and Near Hysteresis-Free Soft Tactile Sensors. *Adv. Mater.* **2022**, *34*, No. 2200682.
(31) Jiang, Y.; An, J.; Liang, F.; Zuo, G.; Yi, J.; Ning, C.; Zhang, H.; Dong, K.; Wang, Z. L. Knitted self-powered sensing textiles for machine learning-assisted sitting posture monitoring and correction. *Nano Res.* **2022**, *15*, 8389−8397.
(32) Lee, H. J.; Yang, J. C.; Choi, J.; Kim, J.; Lee, G. S.; Sasikala, S. P.; Lee, G.-H.; Park, S.-H. K.; Lee, H. M.; Sim, J. Y.; et al. Hetero-dimensional 2D Ti3C2T x MXene and 1D graphene nanoribbon hybrids for machine learning-assisted pressure sensors. *ACS Nano* **2021**, *15*, 10347−10356.
(33) Baek, S.; Lee, Y.; Baek, J.; Kwon, J.; Kim, S.; Lee, S.; Strunk, K.-P.; Stehlin, S.; Melzer, C.; Park, S.-M.; et al. Spatiotemporal Measurement of Arterial Pulse Waves Enabled by Wearable Active-Matrix Pressure Sensor Arrays. *ACS Nano* **2022**, *16*, 368−377.
(34) Goliya, Y.; Rivadeneyra, A.; Salmeron, J. F.; Albrecht, A.; Mock, J.; Haider, M.; Russer, J.; Cruz, B.; Eschlwech, P.; Biebl, E.; et al. Next Generation Antennas Based on Screen-Printed and Transparent Silver Nanowire Films. *Adv. Opt. Mater.* **2019**, *7*, No. 1900995.
(35) Chen, C.; Chen, J.; Han, H.; Chao, L.; Hu, J.; Niu, T.; Dong, H.; Yang, S.; Xia, Y.; Chen, Y.; Huang, W. Perovskite solar cells based on screen-printed thin films. *Nature* **2022**, *612*, 266−271.
(36) Abdolhosseinzadeh, S.; Zhang, C.; Schneider, R.; Shakoorioskooie, M.; Nüesch, F.; Heier, J. A Universal Approach for Room-Temperature Printing and Coating of 2D Materials. *Adv. Mater.* **2022**, *34*, No. 2103660.
(37) Kim, K.-H.; Hong, S. K.; Jang, N.-S.; Ha, S.-H.; Lee, H. W.; Kim, J.-M. Wearable Resistive Pressure Sensor Based on Highly Flexible Carbon Composite Conductors with Irregular Surface Morphology. *ACS Appl. Mater. Interfaces* **2017**, *9*, 17499−17507.
(38) Lo, L.-W.; Shi, H.; Wan, H.; Xu, Z.; Tan, X.; Wang, C. Inkjet-Printed Soft Resistive Pressure Sensor Patch for Wearable Electronics Applications. *Adv. Mater. Technol.* **2020**, *5*, No. 1900717.
(39) Luo, H.; Pang, G.; Xu, K.; Ye, Z.; Yang, H.; Yang, G. A fully printed flexible sensor sheet for simultaneous proximity−pressure−temperature detection. *Adv. Mater. Technol.* **2021**, *6*, No. 2100616.
(40) Bae, K.; Jeong, J.; Choi, J.; Pyo, S.; Kim, J. Large-Area, Crosstalk-Free, Flexible Tactile Sensor Matrix Pixelated by Mesh Layers. *ACS Appl. Mater. Interfaces* **2021**, *13*, 12259−12267.


https://doi.org/10.1021/acsmaterialsau.3c00050
*ACS Mater. Au* 2023, 3, 669−677